Solving the Gain/Coverage Problem to enable 5G-Powered IoT

Aline Eid, Jimmy G.D. Hester, Manos M. Tentzeris

School of Electrical and Computer Engineering
Georgia Institute of Technology
Atlanta, Georgia, USA
aeid7@gatech.edu

Abstract—Mm-wave 5G base-stations are capable of emitting unprecedented EIRPs, necessary to achieve its high data rates. This capability introduces the opportunity to also use this wireless resource to wirelessly power IoT devices. However, the passive recipients of such power densities would need large enough apertures to harvest appropriate power levels to operate, which would naturally limit their angular coverage. In this work, we present an unconventional solution to this problem through the implementation of a passive beamforming network—the Rotman lens—in the receiving mode, as an intermediate element between antenna arrays and rectifiers to enable the surprising combination of high gain and wide angular coverage. The fully-printed, flexible Rotman lens, operating in the mm-wave regime, is equipped with eight antenna ports and six beam ports, selected based on a scalability study. Tested in both planar and bent configurations, the Rotman lens demonstrates a robust, ultra-broadband behavior, with minimum variations in its gain and angular coverage over more than 20 GHz of bandwidth. These structures promise to power the next generation of passive IoT devices at distances exceeding 100 m using 5G base-stations, with the transmission of the full 75 dBm EIRP allowable by the FCC in the 5G/mm-wave bands, thereby enabling the emergence of ultra-low-cost mmIDs for ubiquitous sensing for smart-city and smart-infrastructure applications.

I. INTRODUCTION

Nikola Tesla's dream of wireless power transmission has remained appealing yet elusive and generally impractical due to the fundamental propagation properties of electromagnetic waves. However, the recent developments in mm-wave systems—catalyzed and exemplified by 5G and its high allowed Equivalent Isotropic Radiated Power (EIRP)—have given access to affordable, reasonably-sized high-gain radiators, capable of focalizing their electromagnetic energy to create highly efficient wireless power transfer links. While this high-gain property is very beneficial, it is also a curse for low-cost, large-aperture passive receivers requiring an orientation-agnostic operation. Beamforming networks (BFNs) offer a low-cost, passive solution enabling simultaneous high gains and wide angular coverage. Two widely-known types of circuit-based networks are the Butler matrix and the Blass matrix, that rely on couplers to create phase-shifts between elements, resulting in beam steering in a desired angle. Particularly, Butler matrices have been used for a wide variety of applications, such as phased arrays, MIMO systems, radar systems and energy harvesting [1], [2], [3], [4]. However, these two circuit-based systems suffer from beam squint [5], a characteristic that deteriorates the angular coverage when the frequency of operation deviates from the design frequency. In other words, the beams' angular directions are prone to changes with respect to frequency, which leads to system with limited bandwidths. This phenomenon is quantified in Eq. (1) for the case of the Butler matrix:

$$\Delta\theta_{Butler} = 2\sin^{-1}\left(\frac{c}{2df}\left(1 - \frac{1}{N}\right)\right) \qquad (1)$$

where $\Delta\theta_{Butler}$, c, d, f and N are, respectively, the angular range covered by the Butler BFN, the speed of light, the antenna elements spacing, the frequency of operation and the number of beams.

In addition to its squinting drawback, the architecture of a Butler matrix is relatively complex, especially at higher frequencies where the design parameters (for example, lines lengths less than a quarter wavelength) become extremely critical and difficult to fabricate. A very high design accuracy is required to insure minimum losses in the system and a successful operation at the desired frequency, since the Butler matrix is inherently a narrow-band structure. Wider bandwidths can be achieved with the Bulter matrix network, but at the expense of a more complicated architectures [7], [8]. There is, however, one scanning approach that uses a microwave lens structure to control the relative phase values at the array elements, based on propagation time delays achieving the de-
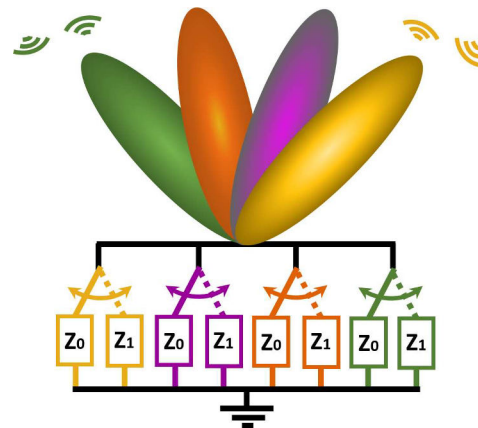

Fig. 1: Schematic of the the Rotman lens-based retrodirective backscatter front end [6].

TABLE I
SCALABILITY STUDY

Parameter (Na,Nb)	Maximum Array Factor	Angular Coverage
(4,3)	1.2 dB	180°
(8,6)	5.95 dB	130°
(16,12)	7.8 dB	100°
(32,24)	7.6 dB	83°
(64,48)	5.2 dB	80°

sired phase gradients. Introduced in the 1960s, the Rotman lens constitutes one of the most cost-effective designs for BFNs and is commonly utilized to enable multibeam phased array system [9] and wide-band operation, thanks to its implementation of true-time-delays. Due to constructive interference, a delay of $\Delta\tau$ between adjacent elements, separated by a distance of d, produces a radiation pattern with an angular coverage expressed by [10]:

$$\Delta\theta_{Rotman} = 2\sin^{-1}\left(\left(\frac{c}{d}\right)\Delta\tau_1\right) \qquad (2)$$

where $\Delta\theta_{Rotman}$, c, d and $\Delta\tau_1$ are, respectively, the angular range covered by the Rotman BFN, the speed of light, the antenna elements spacing and the time delay induced between adjacent elements when port 1 is excited. Since the values of c and d are constant and the beam scan angle depends only on the time delay, $\Delta\tau$, the scanning angle does not vary with frequency, providing that $\Delta\tau$ is independent of frequency (as in transverse-electromagnetic (TEM) transmission media) or is only weakly dispersive (as in so-called quasi-TEM transmission media such as microstrip). In this work, the capabilities of a Rotman lens are demonstrated to enable the surprising combination of high gain and large beamwidth mm-wave coverage for combined energy harvesting and backscattering communications through quasi semi-isotropic RF combining. Because the lens is capable of focusing the energy coming from a given direction into its geometrically-associated beam port, the proposed scheme loads each of these ports with a switch changing between two loads, as shown in Fig. 1, which enables it to either transfer all of the received power to a matched load (for energy harvesting) or to reflect this power with high gain in its direction of arrival, in the case of a purely
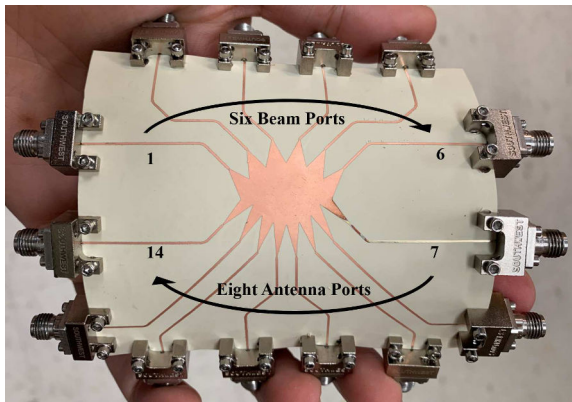
reflective load. In an optimal scenario, if the plane wave is coming from the left direction, the beam port located at the right–that is diametrically opposite to that plane wave–will receive the combined RF power from all antenna elements at the same phase, which translates to a constructive combination of signals. However, unlike other RF combining techniques which fail to achieve this constructive addition for plane waves impinging from directions too far away from broadside, the Rotman lens can be designed such that at least one of the ports benefits from this effect, regardless of the direction of arrival within a large angular range.

II. FLEXIBLE, SCALABLE AND PLANAR MM-WAVE ROTMAN LENS DESIGN

The Rotman lens is surrounded by two angles of curvature, accounting for the antenna ports on one side and the beam ports on the opposite side. The choice of the number of ports of both ends influences the gain, angular coverage and overall performance of the lens and can be tailored for specific applications.

For this application, the Rotman lens is first and foremost expected to have a wide angular coverage and high gain to provide the desired orientation-agnostic energy harvesting and backscattering communications capabilities. Unlike most Rotman lenses, [12], [13], [14], [15], none of the designs used in this work include any impedance-matched dummy ports.
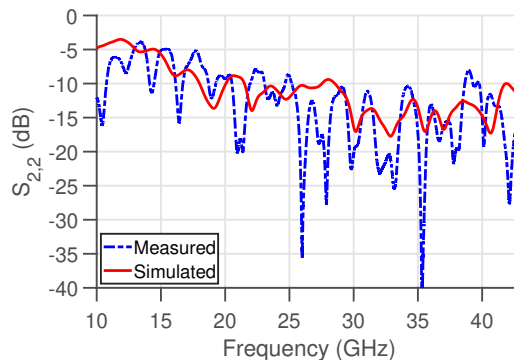
(a)
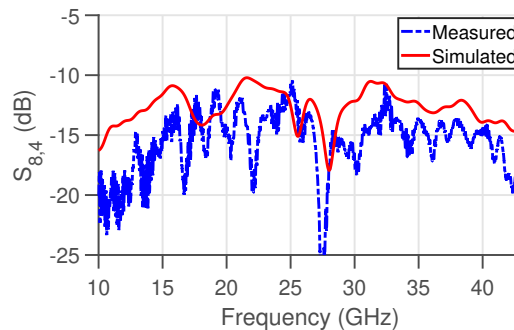
(b)

Fig. 3: (a) Plot of the simulated and measured reflection coefficient at beam port 2 and (b) Plot of the simulated and measured transmission coefficient at antenna port 8 when beam port 4 is excited.

Fig. 2: Picture of the fabricated Rotman lens structure [11].

Their role is to reduce side lobes levels, thereby reducing interference in sensitive communication systems. Their absence does not significantly degrade the levels of the main lobes, but significantly increases the cost of the system by requiring matched loads. Since side lobes are of no concern for this application, these were dispensed with.

In order to gain an understanding of the effects of changing the number of antenna ports and beam ports on the maximum array factor and angular coverage of the lens, structures with different sizes were designed in Antenna Magus and simulated in CST STUDIO. The extracted simulated data was then processed in MATLAB to calculate the array factors and angular coverages for each structure. In table I, the simulated structures with varying number of antenna ports Na and beam ports Nb are displayed. It can be seen that the array factor increases with the increase in the number of antenna ports and beam ports while the angular coverage is decreases. However, for a lens surrounded with more than 16 antenna arrays and 12 beam ports, the array factor starts dropping due to increased complexity and losses caused by internal reflections. Since a structure achieving a combination of good array factor and wide angular coverage is desired, the Rotman lens with 8 antenna ports and 6 beam ports was chosen to be used in this work. The design of the lens was then completed with the addition of tapered lines on both sides to insure smooth impedance transitions from the antennas to the lens as well as from the lens to the beam ports. The fabricated prototype is shown in Fig. 2, fully-printed on flexible $180\,\mu m$ thin Liquid Crystal Polymer substrate (LCP).

The structure was then tested in planar and bent configurations to assess the effects of bending on the reflection and transmission coefficients of the structure. Fig. 3 shows the simulated and measured S parameters of the Rotman lens at specific ports while maintained in an unbent configuration. A good agreement can be observed between the simulated and measured structures over a wide frequency range from $10\,\text{GHz}$ to $43\,\text{GHz}$ with a good matching under $-10\,\text{dB}$ for the reflection coefficients results at beam port 2 ,shown
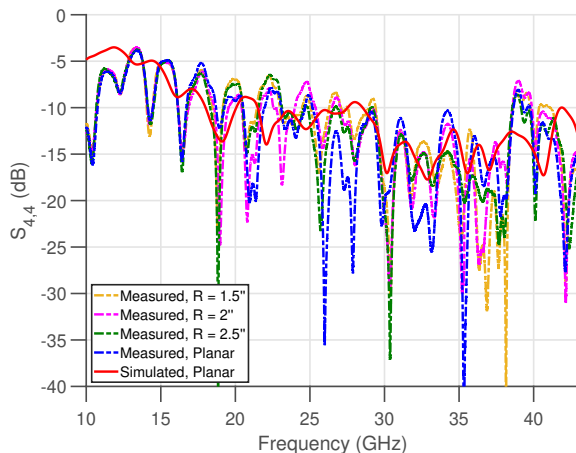

Fig. 4: Plot of the simulated and measured reflection coefficients at beam port 4 under planar and bent conditions [11].
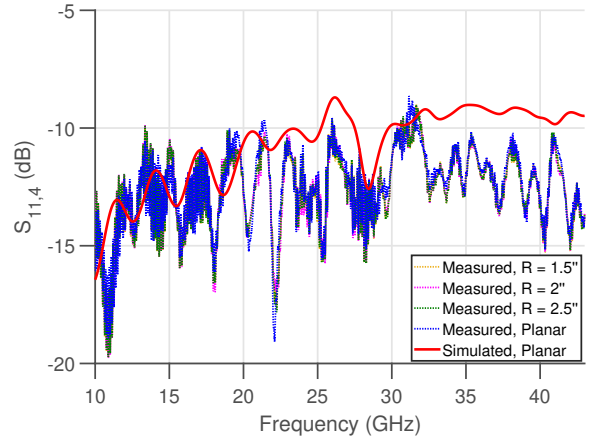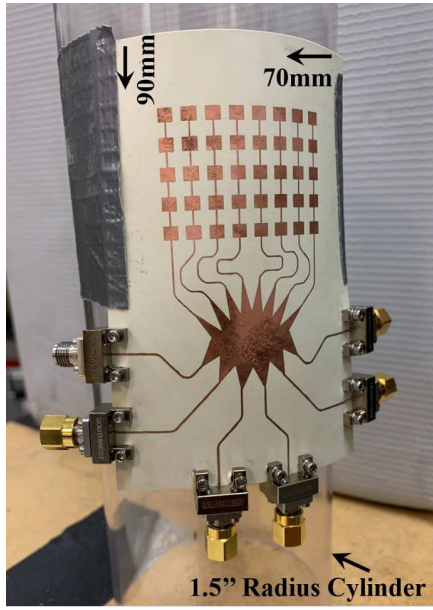

Fig. 5: Plot of the simulated and measured transmission coefficients at antenna port 11 when beam port 4 is excited, under planar and bent conditions.

in Fig. 3a. In addition, a good transmission coefficient is obtained in the most challenging case at antenna port 8– when beam port 4 is excited–as shown in Fig. 3b. One should take into consideration that the power is divided over eight antenna ports, resulting in $9\,\text{dB}$ loss in power in lossless, perfect conditions. The S parameters were then evaluated under bending by placing the Rotman lens on cylinders of different sizes, ranging from 1.5 to 2.5 inch in radii. Fig. 4 and Fig. 5 show the measured reflection and transmission responses between beam port 4 and antenna port 11 for four different scenarios, compared to the simulated planar structure. The results show that the Rotman lens is able to maintain a stable matching with minor losses—compared to being held in a planar position—while being mounted on curved surfaces down to a radius of R = 1.5". This result also validates the robustness and performance stability of the Rotman lens under extreme wrapping, bending, and folding, as presented in previous works [16], [17].

III. HIGH GAIN AND WIDE BEAMWIDTH ROTMAN LENS-BASED ANTENNA ARRAY

The design of the Rotman lens-based antenna array was completed with the addition of eight linear antenna arrays, introduced in [18], each consisting of five serially-fed patch antennas, operating in the $28\,\text{GHz}$ band with a reflection coefficient S_{11} lower than $-20\,\text{dB}$ within this range. With an E-plane beamwidth of about $18°$, the antenna array is suitable for most use cases, where environments expand mostly horizontally. It has a simulated gain of $13\,\text{dBi}$ and a H-plane beamwidth of $80°$ in the plane perpendicular to the linear array. In this implementation, a six-beams configuration, with them intersecting at angles providing 3dB lower gain than broadside, was chosen. Eight antennas each providing a 3dB-beamwidth of $18°$ were utilized, thereby covering a total of $6\times18° = 108°$ in front of the array. Fig. 6ashows the inkjet-printed, planar and flexible Rotman lens-based antenna array, mounted on an 1.5" radius cylinder.

(a)
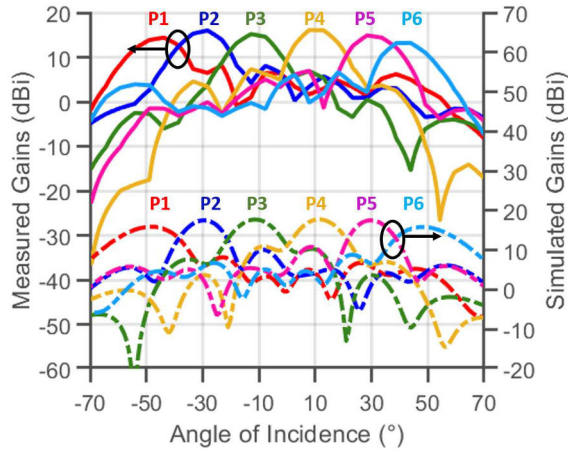
(b)

Fig. 6: (a) Plot of the simulated and measured reflection coefficient at beam port 2 and (b) Plot of the simulated and measured transmission coefficient at antenna port 8 when beam port 4 is excited [11].

The radiation properties and gain of the structure were studied next. The radiation patterns of the lens-based antenna system were simulated using the time-domain solver of CST STUDIO and the gain at every port was also accurately measured using a $20\,\mathrm{dBi}$ transmitter horn antenna and by terminating all five remaining ports with a $50\,\Omega$ load for every port measurement to guarantee the proper operation of the lens. The losses introduced by the additional microstrip lines necessary to provide enough space for the interfacing $2.9\,\mathrm{mm}$ connectors were, however, not accounted for. The true gain of the lens therefore is likely higher than the one displayed in the figure by 1 to $2\,\mathrm{dB}$. The simulated and measured radiation patterns are both displayed in Fig. 6b, displaying a remarkable agreement with a measured gain of approximately $17\,\mathrm{dBi}$, and

an angular coverage of around $110°$, thereby validating the operation of the Rotman lens-based antenna array. The same measurement was also performed while bending the structure over a curvature of 1.5" radius, and the gains on the first three ports were measured and compared to the measured results on a planar surface. The antenna array maintained a stable gain—particularly over the center beams—with a minor deterioration in the received power at the beams located at the edges [11]. The realized combination of high gain and angular coverage of this Rotman-based antenna array has enabled the development of long-range efficient 5G/mm-wave energy harvesting, with the addition of rectifiers at the beam ports, achieving a 21-fold increase in harvested power compared to a lensless rectenna by RF-combining all of the power impinging from a given direction to a single rectifier. This breakthrough in mm-wave energy harvesting, allowing an orientation agnostic collection of the 5G signals, promises to power IoT devices at ranges exceeding $100\,\mathrm{m}$ [11]. The implementation of the Rotman lens-based antenna array was not limited to wireless power transfer applications, but was also used as a retrodirective array, demonstrating ultra-low power and km-range backscattering communications, realized with the addition of switches at its beam ports [6].

IV. Conclusion

The work reported in this paper extends landmark efforts introducing the use of unconventional Rotman-lens-based mmID structures for the ultra-long-range powering and ultra-low-power communication of passive devices using mm-wave 5G infrastructure by characterizing the behavior of such circuits under stringent bending conditions and demonstrating their incredible robustness. These results further strengthen the case for the practical applicability of Rotman-lens-based passive IoT sensors for ubiquitous deployments in smart city and smart infrastructure systems.

References

[1] A. Grau, J. Romeu, S. Blanch, L. Jofre, and F. De Flaviis, "Optimization of linear multielement antennas for selection combining by means of a butler matrix in different mimo environments," *IEEE Transactions on Antennas and Propagation*, vol. 54, no. 11, pp. 3251–3264, 2006.

[2] G. Tudosie, H. Barth, and R. Vahldieck, "A compact ltcc butler matrix realization for phased array applications," in *2006 IEEE MTT-S International Microwave Symposium Digest*. IEEE, 2006, pp. 441–444.

[3] S. Y. Nusenu, S. Huaizong, P. Ye, W. Xuehan, and A. Basit, "Dual-function radar-communication system design via sidelobe manipulation based on fda butler matrix," *IEEE Antennas and Wireless Propagation Letters*, vol. 18, no. 3, pp. 452–456, 2019.

[4] Y. Wang and K. Ma, "A novel self-packaged sisl butler matrix for automotive radar application," in *2017 IEEE MTT-S International Microwave Workshop Series on Advanced Materials and Processes for RF and THz Applications (IMWS-AMP)*. IEEE, 2017, pp. 1–3.

[5] R. L. Haupt, *Timed arrays: wideband and time varying antenna arrays*. John Wiley & Sons, 2015.

[6] A. Eid, J. G. D. Hester, and M. M. Tentzeris, "Rotman lens-based wide angular coverage and high-gain semipassive architecture for ultralong range mm-wave rfids," *IEEE Antennas and Wireless Propagation Letters*, vol. 19, no. 11, pp. 1943–1947, 2020.

[7] K. Wincza and K. Sachse, "Broadband 4×4 butler matrix in microstrip multilayer technology designed with the use of three-section directional couplers and phase correction networks," in *18-th International Conference on Microwaves, Radar and Wireless Communications*. IEEE, 2010, pp. 1–4.

[8] T.-H. Lin, S.-K. Hsu, and T.-L. Wu, "Bandwidth enhancement of 4× 4 butler matrix using broadband forward-wave directional coupler and phase difference compensation," *IEEE Transactions on Microwave Theory and Techniques*, vol. 61, no. 12, pp. 4099–4109, 2013.

[9] K. Wang, J.-F. Gu, F. Ren, and K. Wu, "A multitarget active backscattering 2-d positioning system with superresolution time series post-processing technique," *IEEE Transactions on Microwave Theory and Techniques*, vol. 65, no. 5, pp. 1751–1766, 2017.

[10] M. GLEAVES, "Rotman lens' electronic beam steering aims at 5g signals."

[11] A. Eid, J. G. Hester, and M. M. Tentzeris, "5g as a wireless power grid," *Scientific Reports*, vol. 11, no. 1, pp. 1–9, 2021.

[12] A. Attaran, R. Rashidzadeh, and A. Kouki, "60 ghz low phase error rotman lens combined with wideband microstrip antenna array using ltcc technology," *IEEE Transactions on Antennas and Propagation*, vol. 64, no. 12, pp. 5172–5180, 2016.

[13] M. A. Hassanien, R. Hahnel, and D. Plettemeier, "Wideband rotman lens beamforming technique for 5g wireless applications," in *2019 2nd International Conference on Computer Applications & Information Security (ICCAIS)*. IEEE, 2019, pp. 1–5.

[14] K. Tekkouk, M. Ettorre, and R. Sauleau, "Siw rotman lens antenna with ridged delay lines and reduced footprint," *IEEE Transactions on Microwave Theory and Techniques*, vol. 66, no. 6, pp. 3136–3144, 2018.

[15] N. Jastram and D. S. Filipovic, "Design of a wideband millimeter wave micromachined rotman lens," *IEEE Transactions on Antennas and Propagation*, vol. 63, no. 6, pp. 2790–2796, 2015.

[16] A. Rahimian, Y. Alfadhl, and A. Alomainy, "Design and performance of a flexible 60-ghz rotman lens-based array beamformer," in *12th European Conference on Antennas and Propagation (EuCAP 2018)*. IET, 2018, pp. 1–2.

[17] T. K. Vo Dai and O. Kilic, "Compact rotman lens structure configurations to support millimeter wave devices." *Progress in Electromagnetics Research B*, vol. 71, 2016.

[18] A. Eid, J. Hester, and M. M. Tentzeris, "A scalable high-gain and large-beamwidth mm-wave harvesting approach for 5g-powered iot," in *2019 IEEE MTT-S International Microwave Symposium (IMS)*, June 2019, pp. 1309–1312.